Quantum Electronics **41** (6) 557–563 (2011)

BIOPHOTONICS

PACS numbers: 42.25.Fx; 87.64.Cc; 87.55.K–
DOI: 10.1070/QE2011v041n06ABEH014642

Visualisation of structural inhomogeneities in strongly scattering media using the method of spatially-resolved reflectometry: Monte Carlo simulation

A.V. Bykov, A.V. Priezzhev, R. Myllylä

Abstract. **Two-dimensional spatial intensity distributions of diffuse scattering of near-infrared laser radiation from a strongly scattering medium, whose optical properties are close to those of skin, are obtained using Monte Carlo simulation. The medium contains a cylindrical inhomogeneity with the optical properties, close to those of blood. It is shown that stronger absorption and scattering of light by blood compared to the surrounding medium leads to the fact that the intensity of radiation diffusely reflected from the surface of the medium under study and registered at its surface has a local minimum directly above the cylindrical inhomogeneity. This specific feature makes the method of spatially-resolved reflectometry potentially applicable for imaging blood vessels and determining their sizes. It is also shown that blurring of the vessel image increases almost linearly with increasing vessel embedment depth. This relation may be used to determine the depth of embedment provided that the optical properties of the scattering media are known. The optimal position of the sources and detectors of radiation, providing the best imaging of the vessel under study, is determined.**

Keywords: *optical methods of imaging, spatially-resolved reflectometry, scattering, Monte Carlo simulation.*

1. Introduction

At present different versions of spectroscopy and imaging methods, based on detecting the radiation diffusely reflected from biological tissues, are the subject of intent studies [1], aimed at determining the spatial distributions of the optical parameters of the media under study. Rigorous determination and monitoring of the variation in these distributions may provide physiologically valuable information, e.g., on the presence of a hematoma or on the location of a blood vessel. Depending on the type of probing radiation and the scattered radiation detection regime in the experiment and simulation cw, time-domain and frequency-domain (modulation) techniques of measurement are used [2]. In the present paper, we study the capabilities of the spatially-resolved reflectometry (SRR) method, in which a cw near-infrared laser radiation is used for imaging and determining the characteristic size and depth of embedment of one or a few static cylindrical inhomogeneities, simulating blood vessels, submerged into a scattering medium, mimicking skin.

The essence of the SRR method consists in measuring the dependence of the intensity of radiation, scattered by the medium into the back semispace, on the distance r between the source and the detector. We will refer to this dependence as a SRR signal. In the present method, the monochromatic radiation is directed onto the studied medium through an optical fibre of definite diameter. The backscattered radiation is usually measured using a linear array of detectors mounted along a certain line on the same medium surface, as the radiation source, or by stepwise moving a single detector along this line. As a rule, fibreoptical detectors are used in modern systems, so that the measuring head directly contacting the studied object is implemented as a set of optical fibres with chosen diameters and numerical apertures. In the cases, when the two-dimensional SSR signals are to be obtained from a large area of the sample, CCD-arrays are used [3]. For portable sensors, one can make use of infrared light-emitting diodes, which are much cheaper than lasers, and place them on a single chip with the detectors of radiation. A general schematic diagram of such device is presented in Fig. 1.

The analysis of radiation propagation in scattering media on the basis of the diffusion theory shows that in the present case the most probable trajectories of photons reaching the

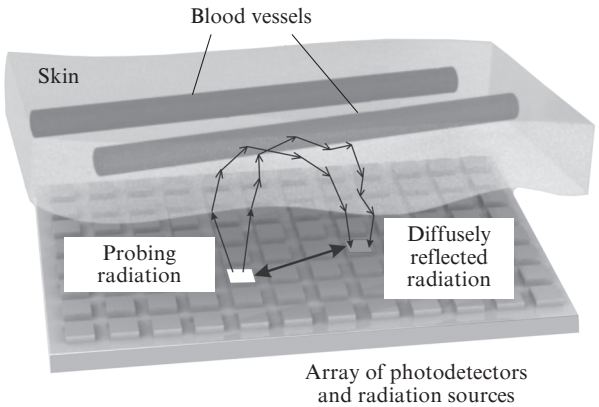

Figure 1. General schematic diagram of the setup for imaging structural inhomogeneities in a scattering medium using the SRR method.

A.V. Bykov Department of Physics, M.V. Lomonosov Moscow State University, Vorob'evy gory, 119992 Moscow, Russia; present address: University of Oulu, Optoelectronics and Measurement Techniques Laboratory, P.O. Box 4500, 90014 University of Oulu, Finland; e-mail: bykov@ee.oulu.fi;
A.V. Priezzhev Department of Physics, M.V. Lomonosov Moscow State University, Vorob'evy gory, 119992 Moscow, Russia; e-mail: avp2@mail.ru;
R. Myllylä University of Oulu, Optoelectronics and Measurement Techniques Laboratory, P.O. Box 4500, 90014 University of Oulu, Finland; e-mail: risto.myllyla@ee.oulu.fi

Received 18 April 2011
Kvantovaya Elektronika **41** (6) 557–563 (2011)
Translated by V.L. Derbov

detector are spatially limited to a domain having a banana-like shape [4, 5]. The curve describing the domain of the most probable trajectories has an extremum at the distance $r/2$ from the source. The maximal depth z_{max} in case of weak absorption is given by the formula $z_{max} = \sqrt{2}r/4$ [5]. This parameter can be used to estimate the maximal penetration depth of radiation into the scattering medium when using the SRR method.

The SRR method allows one to determine not only optical parameters of the medium averaged over the whole sample but also the optical properties of each layer of a stratified medium [6]. This method is definitely preferable for noninvasive diagnostics, because the source and the detector are located on the same side of the medium under study. Analytical description of the SRR signal is possible in simple particular cases or using approximations [7]. The analytical solution exists also for a two-layer medium in the diffusion approximation [8], but it is rather cumbersome. As in many other fields of biotissue optics, the use of the Monte Carlo method appears to be one of the efficient means to simulate the SRR signal [9, 10]. We have significant experience in using this method to describe different problems of propagation of laser radiation in strongly scattering media and in simulating the signals in various optical devices [11–13].

The SRR method can be also used to image structural inhomogeneities of the medium under study. Thus, e.g., in [14] a measuring head was designed to image the forearm blood vessels. The device included a fibreoptical source and a detector, fixed at a definite distance from each other, and was used to scan the forearm surface. Encoding by colour the distributions of the measured power, the authors obtained the image of the vascular structure of the studied area. The experimental studies have demonstrated the potential of this method to be used in monitoring the state of biotissues and blood circulation, as well as the blood oxygen content.

In Ref. [15] another version of measuring head is presented, consisting of several source–detector pairs placed at an angle to each other to form a star. As shown earlier by the same authors [16], with the use of a special algorithm for processing the measured signal, this approach allows one to improve the spatial resolution of the diffusion method. In Ref. [15] it is shown that the application of such a scanning system also allows one to differentiate the vessels with respect to the depth of their embedment.

The SRR technique may be also used for monitoring the activity of the brain cortex [17, 18] and for detecting the hematomas [19, 20]. The studies performed have shown that the brain activity leads to a change in its tissue optical properties [18] and manifests itself in a change in the blood volume, degree of oxygenation, and the ratio of oxy- and deoxyhemoglobin, which causes a change in absorption and scattering coefficients, detected by the SRR method. In neurology, the optical methods are still rarely used, since their resolution and probing depth are worse than those of other functional brain imaging methods, such as nuclear magnetic resonance tomography and positron emission tomography. However, the optical methods and related instruments possess some advantages, e.g., portability (allowing one to conduct the measurements even on a walking human) and sensitivity to biochemical processes (allowing for the determination of concentration of such substances as oxy- and deoxyhemoglobin). Not the least of the practical aspects is potentially lower cost of SRR-based devices.

In the present paper, a numerical study of potential capabilities of the SRR method is carried out in respect of designing a simple and reliable device for noninvasive diagnostics of large-scale inhomogeneities of a biological tissue, such as blood vessels, as well as for determination of their shape, size and position.

2. Modelled experiment

Consider the case when an inhomogeneity (a cylinder-shaped blood vessel) is submerged into a scattering medium parallel to its surface at a certain depth. Let us choose a cw near-infrared laser (λ = 820 nm) as a source of radiation. A schematic diagram of the modelled experiment is presented in Fig. 2. Bold arrow shows the probing beam entering the medium in the Z axis direction at the point $(0, 0, 0)$ normally to the medium surface XY. The transverse dimensions of the beam are considered to be negligibly small for simplicity, although this assumption in not a matter of principle. The vessel centre is positioned directly under the point where the beam enters the medium. The embedment depth of the blood vessel z_{cyl} varied from 1 to 5 mm, the vessel radius R was chosen to be 0.5 mm. The medium, surrounding the vessel, has the shape of a rectangular parallelepiped with the dimensions $x = y = 50$ mm, $z = 20$ mm.

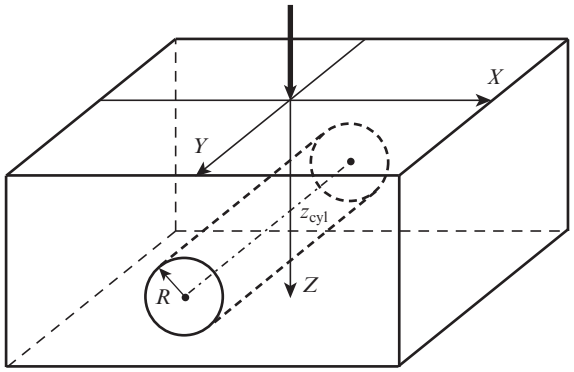

Figure 2. Schematic diagram of the medium used in the MC simulation: a cylindrical inhomogeneity with the radius R simulating a blood vessel is submerged into 2% intralipid layer at the depth z_{cyl}.

The simulation of the process of propagation of laser radiation was performed using the MC method [9]. For this purpose the algorithm for simulation of the process of propagation of laser radiation in stratified media implemented by us earlier on a parallel-architecture computer [11] was modified with a cylindrical inclusion taken into account.

The blood in the vessel was considered as a suspension of non-aggregating red blood cells with hematocrit (volumetric concentration) of 35%. This concentration is close to the physiological concentration of red blood cells in the human blood filling small vessels. 2% intralipid solution was used to mimic the surrounding medium. At the given concentration, this solution has the scattering properties, close to those of skin, and is often used in experiments to mimic it [21]. Intralipid is a polydisperse suspension of lipid particles (droplets of soybean oil, coated with lipid membrane 2.5–5 nm thick) of practically spherical shape with the mean radius of ~0.3 μm suspended in glycerol or aqueous solution [22–24].

The optical parameters of blood and intralipid (the scattering coefficient μ_s, the absorption coefficient μ_a, the anisotropy factor g, and the refractive index n) at the wavelength

Table 1. Optical parameters of the studied media.

Medium	λ/nm	μ_s/mm^{-1}	μ_a/mm^{-1}	g	n	l^*/mm	l/mm	μ_s'/mm^{-1}
Blood (35%)	820	57.3	0.82	0.977	1.4	0.47	0.02	1.32
Intralipid (2%)	820	5.4	0.002	0.7	1.36	0.62	0.19	1.62

820 nm are presented in Table 1. The data for blood were taken from Ref. [25]; for intralipid the data were recalculated from the known data for its 10% concentration [22–24] under the assumption that the scattering coefficient is linearly dependent on the concentration, while the phase function and the anisotropy factor remain constant. Such assumption is valid because the considered concentrations of intralipid are relatively low. In Table 1 we also present the values of mean transport pathlength $l^* = (\mu_s' + \mu_a)^{-1}$, mean free pathlength $l = \mu_s^{-1}$ and reduced scattering coefficient $\mu_s' = \mu_s(1 - g)$ for the chosen media.

The wavelength of probing radiation $\lambda = 820$ nm is within the so-called diagnostic transparency window of biotissues (600–1300 nm) and is often used in their noninvasive diagnostics.

The detectors of diffusely reflected radiation are placed in the cells of a two-dimensional net placed on the surface xy of the studied medium. The cell dimensions are $\Delta x = \Delta y = 200$ μm. The numerical aperture of each detector is equal to 0.33. Each intensity distribution of the diffusely scattered radiation (2D SRR signal) over the medium surface was obtained by calculating the trajectories of 10^9 photons, launched into the medium. The computation time was ~200 min using 100 processors for the medium with dimensions 50×50×20 mm. Such a long time taken to solve the direct problem is determined by the large (6.25×10^4) number of small detectors, which is necessary to provide high spatial resolution at the stage of investigating the basic features of this imaging technique.

3. Results and discussion

3.1. Imaging a cylindrical blood capillary in a strongly scattering medium with the help of the SRR method

The results of spatially-resolved calculation of the intensity of radiation diffusely reflected from a strongly scattering medium mimicking skin with a blood vessel at the depth of 1 mm and without a vessel, are presented in Fig. 3. It is seen that the intensity of diffusely reflected radiation quickly decreases with distance from the source (point $x = y = 0$). Due to high coefficients of scattering and absorption of the medium filling the vessel, the intensity decrease is the most essential in the area located directly above the vessel, which makes it possible to image the vessel and observe its shape.

Similar calculations were performed for greater vessel depths of embedment ($z_{cyl} = 1$–5 mm). To analyse the influence of the vessel on the signal in this case we calculated the difference of SRR signals $I(x, y)$ from the medium with the vessel at variable depth and $I_0(x, y)$ from a homogeneous medium containing no blood vessel (Fig. 4). The presence of a dark spot in the centre of the picture is explained by the fact that the blood vessel being placed at a certain depth, from 1 mm and deeper, does not significantly affect the reflected radiation, when calculating the SRR signal at small distances from the source. The quantities I_0 and I appear to be close to each other and, therefore, the difference $I - I_0$ becomes minimal, causing the appearance of the dark spot. This is also the reason why the spot size increases with increasing the embedment depth of vessel. When the depth of the vessel embedment increases, the vicinity of the source, within which the medium may be considered as homogeneous and the difference $I - I_0$ is close to zero, becomes larger.

Next we averaged the difference $I - I_0$ over the Y axis (along the vessel) (Fig. 5a). It is seen that due to multiple scattering the image of the vessel blurs with the growth of the depth of its embedment. To characterise this blurring, the half-width $\Delta_{0.5}$ of the quantity $\langle I - I_0 \rangle$ at the half-maximum level is used (Fig. 5b). It is seen that with the growth of the embedment depth of vessel the quantity $\Delta_{0.5}$ grows linearly. This fact allows an unambiguous determination of the embedment depth of the vessel of the known diameter in the medium with known optical properties.

To determine the optimal point of radiation entry we also studied the influence of the source position on the intensity with respect to the vessel on the intensity of the signal, diffusely reflected from the medium. For one of the depths ($z_{cyl} = 1.5$ mm) we calculated the 2D SRR signals at different positions of the source on the X axis: $x = 0$, 0.5, 1.5, 5, and 10 mm at $y = 0$. The results of the calculations are shown in Fig. 6. It is seen that the dark spot reduces its size and vanishes as the source

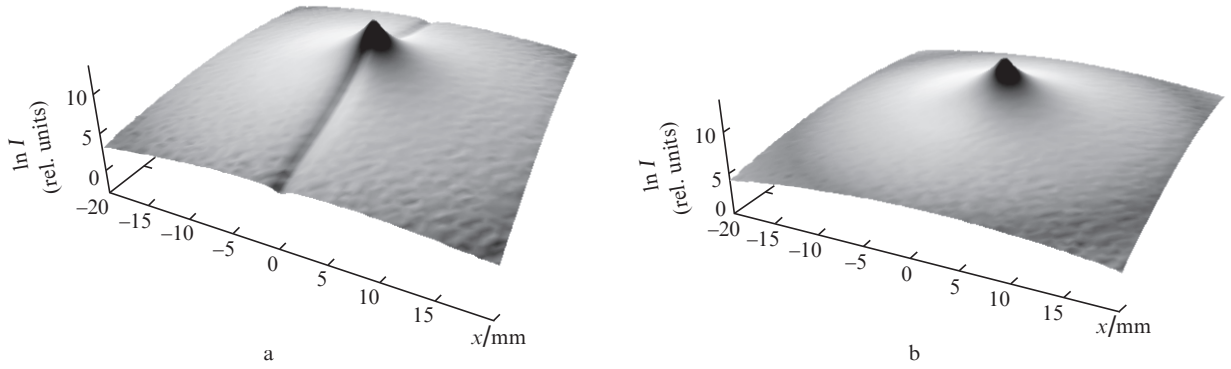

Figure 3. Surface distribution of the intensity I of radiation diffusely reflected from a strongly scattering medium with a cylindrical blood vessel having the radius $R = 0.5$ mm located at the depth $z_{cyl} = 1$ mm (a), and without a vessel (b).

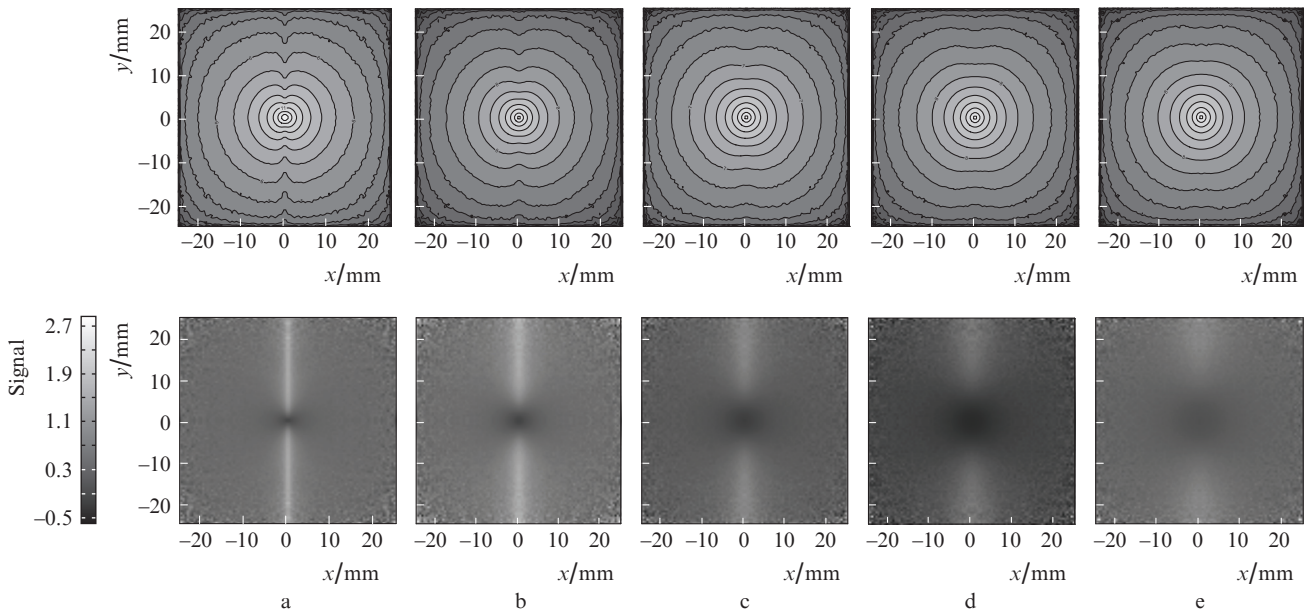

Figure 4. Contour plots of two-dimensional SRR signal $I(x,y)$ in the presence of a cylindrical blood vessel with the radius $R = 0.5$ mm at the variable depth z_{cyl} in the medium (top) and greyscale maps of the difference between the SRR signal $I(x,y)$ and the signal $I_0(x,y)$, recorded from a homogeneous medium, containing no vessels; $z_{cyl} = 1$ (a), 2 (b), 3 (c), 4 (d), and 5 mm (e) (bottom).

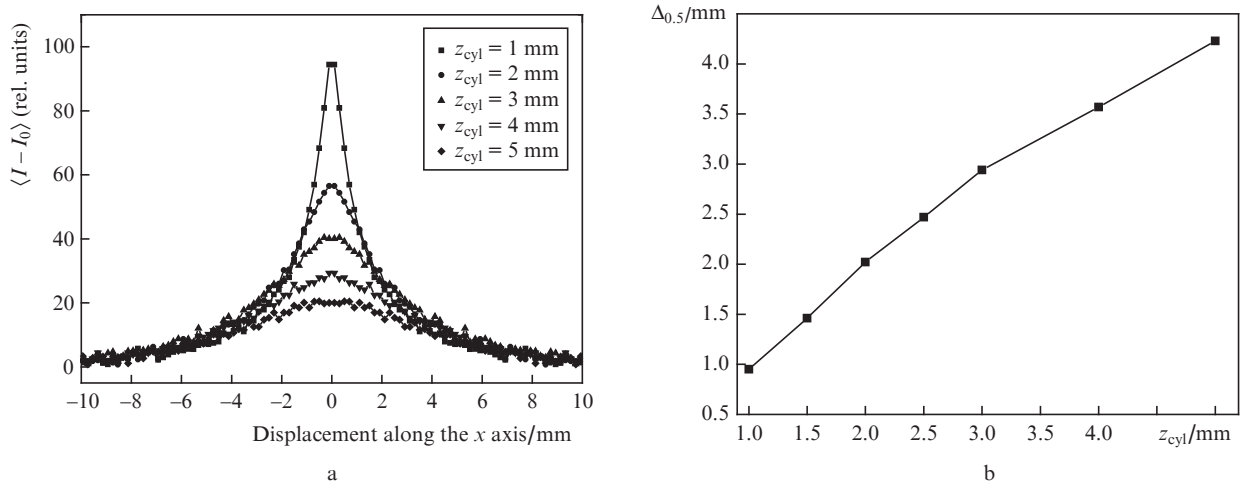

Figure 5. The values of $\langle I - I_0 \rangle$ for different blood vessel depths of embedment z_{cyl} (a) and the dependence of the half-maximum half-width $\Delta_{0.5}$ of the quantity $\langle I - I_0 \rangle$ on z_{cyl} (b).

is moved along the X axis. However, as known, the signal-to-noise ratio decreases with increasing distance between the source and the detector, and, therefore, the vessel image becomes noisy, because it is formed by SRR signals, containing a growing noise component. These two competing effects (the appearance of the spot and the noisy image) determine the optimal position of the source. Hence, it is possible to consider the case in Fig. 6d as corresponding to the optimal position.

In analogy with the mentioned above, the quantity $\langle I - I_0 \rangle$ was also calculated for different positions of the source on the X axis (Fig. 7). It is clearly seen that simultaneously with the source displacement a definite broadening of the left half of the curve occurs. Therefore, to determine correctly the value of $\Delta_{0.5}$ one should use the right part of the curve or introduce correction factors for the left one. It is also worth noting that moving the source away from the studied vessel leads to an increase in the error in determining $\Delta_{0.5}$, which, in turn, may increase the error in the determined embedment depth of this vessel.

A logical development of the proposed technique of the vessel imaging aimed at improving the image quality is to use several sources placed symmetrically with respect to the studied object. Thus, Fig. 8a presents the surface intensity distribution of radiation, diffusely reflected from the scattering medium with a blood vessel, submerged at the depth $z_{cyl} = 1.5$ mm, being probed with two sources, placed at the points $x = \pm 5$, $y = 0$. The total number of the launched photons remains the same, i.e., the power of each source is equal to a half of the power of the source, used above. The image of the vessel, constructed by finding the difference between the SRR signals from the medium with the vessel and without it, for this case is presented in Fig. 8b. From the comparison of Figs. 8b and c it is seen that the use of two sources allows for the improvement of the vessel image quality and makes the image more

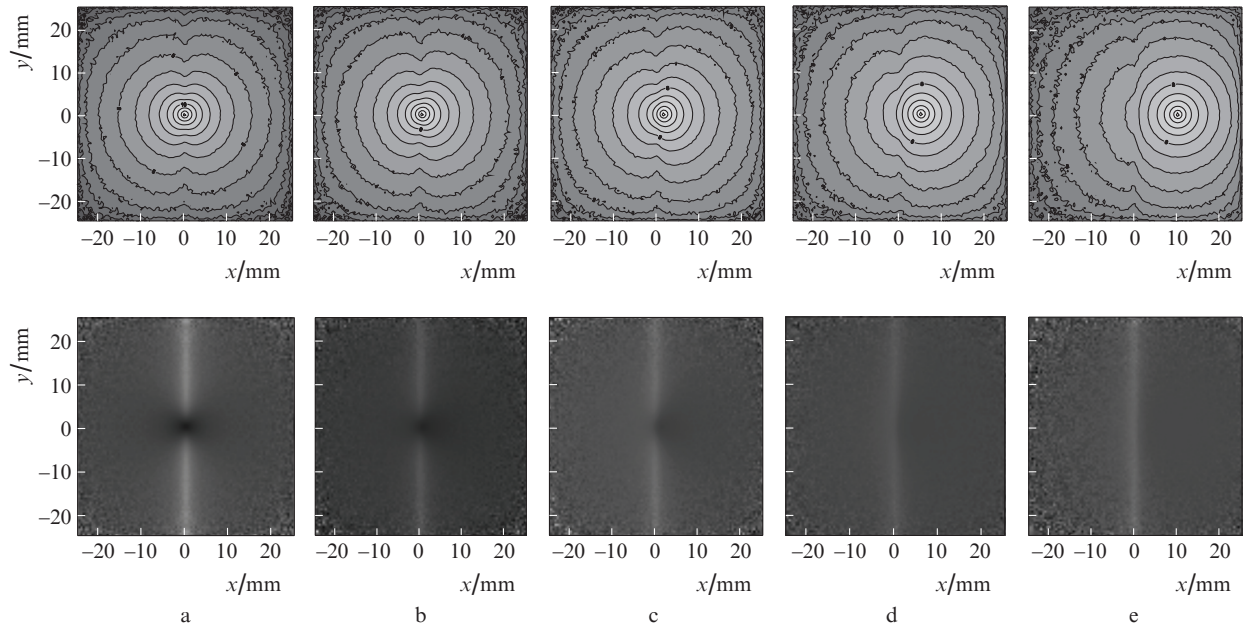

Figure 6. Contour plots of the two-dimensional SRR signal $I(x,y)$ in the presence of a cylindrical blood vessel (R = 0.5 mm, z_{cyl} = 1.5 mm) for different distances x between the point of the photon entry and the centre of the vessel (top), and greyscale maps of the difference between the SRR signals $I(x,y) - I_0(x,y)$ at x = 0 (a), 0.5 (b), 1.5 (c), 5 (d), and 10 mm (e) (bottom).

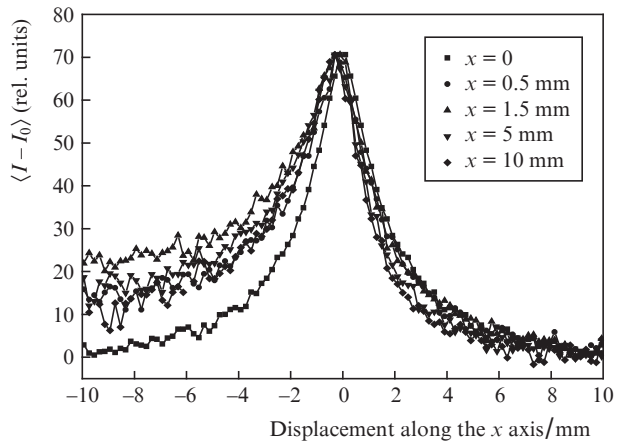

Figure 7. The values of $\langle I - I_0 \rangle$ for the blood vessel with the radius R = 0.5 mm, placed at the depth z_{cyl} = 1.5 mm depending on the distance x between the point of photon entry and the centre of the medium.

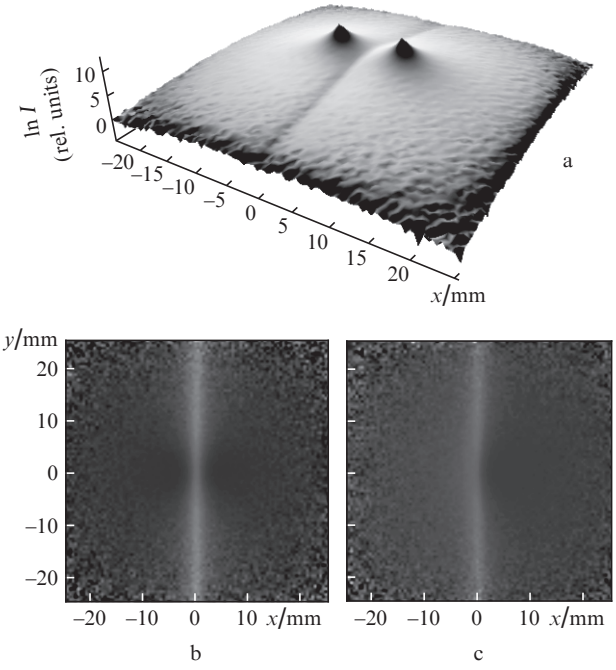

Figure 8. Surface distribution of the intensity of radiation, diffusely reflected from the scattering medium with a cylindrical vessel having the radius R = 0.5 mm and placed at the depth z_{cyl} = 1.5 mm probed with two sources (a) and the images of the same vessel probed with two sources placed at the points $x = \pm 5$ mm, y = 0 (b), and a single source placed at the point x = 5 mm, y = 0 (c).

distinct as compared to the case of a single source having the power, equal to the sum of powers of the two sources. This becomes even more evident when comparing the values of $I - I_0$, averaged over the Y axis, for the cases of medium probing with one and two sources. The curve $\langle I - I_0 \rangle = f(x)$ becomes symmetric again, and its left part – less noisy.

3.2. Maximal imaging depth

The considered technique allows for the solution of the problem about the maximal depth of the vessel embedment z_{cyl}^{max}, at which its imaging is still possible. Obviously, this depth must depend on the vessel radius. Therefore, the calculations were carried out for the radius values of 0.25, 0.5, 0.75, and 1 mm (Fig. 10). The maximal depth z_{cyl}^{max} was determined as the depth of the vessel embedment, at which the noise level of the curve $\langle I - I_0 \rangle = f(x)$ became equal to its maximal value. From Fig. 10 it follows that the vessel having the radius R = 0.25 mm can be observed up to the depth of 2 mm, while the vessel with the radius 1 mm is observable up to the depth of 8 mm. It should be also emphasised that in a real biotissue the maximal depth of imaging may be less than the calculated one because of greater absorption in the medium surrounding the vessel and

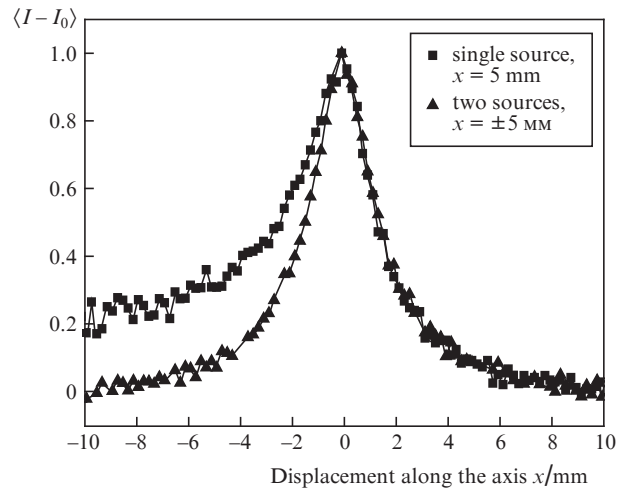

Figure 9. Normalised values of $\langle I - I_0 \rangle$ for the blood vessel having the radius $R = 0.5$ mm placed at the depth $z_{cyl} = 1.5$ mm under two regimes of probing the studied medium.

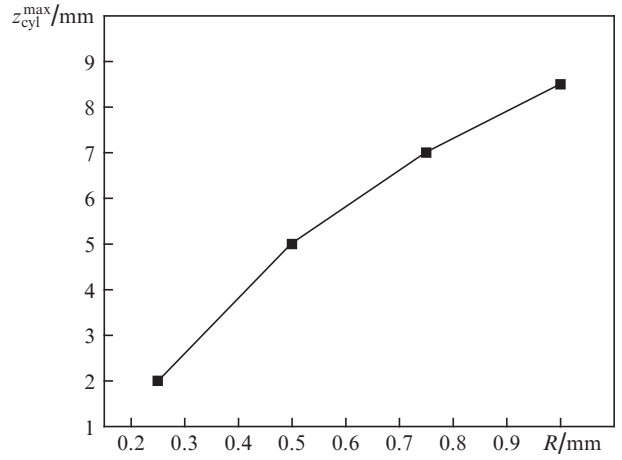

Figure 10. Dependence of the maximal depth of the vessel embedment, at which it is still possible to image it using the SRR method, on the radius of the vessel.

the presence of capillary plexuses, which inevitably lead to the reduction of the image contrast. It is possible to compensate for this disadvantage or even increase the maximal imaging depth using special dyes, added to the blood [26], in combination with the biotissue optical clearing technique [27].

3.3. Determination of the vessel radius and of its embedment depth

Aimed at studying the possibility to use the SRR technique for determining the radius and the depth of embedment of the vessel, we performed calculations of the signal for several values of R and z_{cyl}. The distributions $\langle I - I_0 \rangle$ for $R = 0.5$ and 0.75 mm at the depths of embedment 1 and 5 mm are presented in Fig. 11a. With the increasing radius of the vessel the peak value of $\langle I - I_0 \rangle$ grows at the constant depth of embedment, which leads to an increase in the contrast of the vessel image. However, the increase in R does not cause any essential changes in $\Delta_{0.5}$ for the difference $\langle I - I_0 \rangle$ at any of the considered depths (Fig. 11b). The dependence of the peak value of $\langle I - I_0 \rangle$ on the depth of embedment of the vessel is

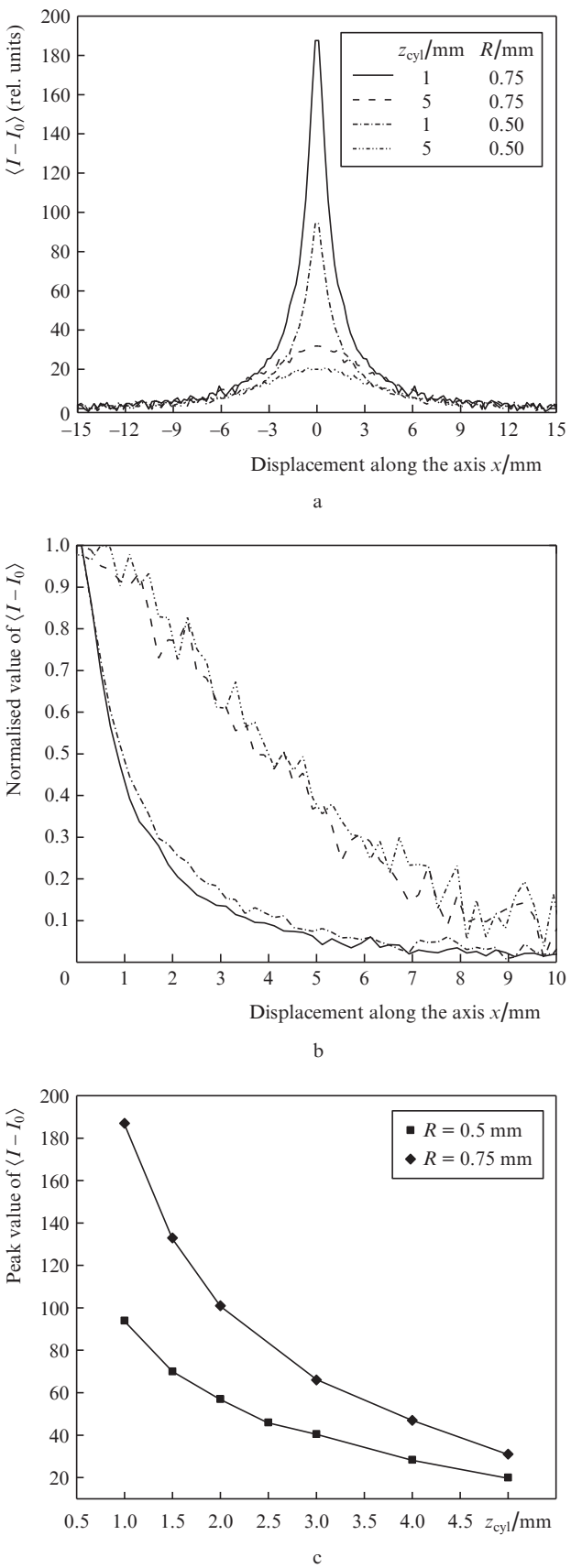

Figure 11. Distribution of $\langle I - I_0 \rangle$ at different depths of embedment of a cylindrical blood vessel with $R = 0.5$ and 0.75 mm (a), normalised values of $\langle I - I_0 \rangle$ for the same cases (b), and dependences of the peak value of $\langle I - I_0 \rangle$ on the depth of the vessel embedment at $R = 0.5$ and 0.75 mm (c).

shown in Fig. 11c. It is seen that this parameter is sensitive to the change in the vessel radius; the sensitivity exhibits the maximal value at small depths, and then monotonously decreases with an increase in z_{cyl}.

Thus, provided that the optical properties of the cylindrical vessel itself and the medium surrounding it are known, we have two parameters obtained from experiment for determining the radius of the cylinder and the depth of its embedment. They are the peak value of $\langle I - I_0 \rangle$ and the half-width $\Delta_{0.5}$. The numerical calculation shows that $\Delta_{0.5}$ is practically independent of the cylinder radius in the considered range of its values. Therefore, from this quantity one can unambiguously determine the depth of the vessel embedment using the curve in Fig. 5b. The second parameter (the peak value of $\langle I - I_0 \rangle$) appears to be dependent on both sought parameters; however, one of them (z_{cyl}) is already known. Determination of the vessel radius at known z_{cyl} is possible on the basis of the calculated curves in Fig. 11c.

4. Conclusions

In the present work, using Monte Carlo method we obtained the realisations of the model spatially-resolved reflectometry signal from a cylindrical vessel, filled with a substance having the optical parameters, characteristic for a suspension of non-aggregating red blood cells, and submerged into a scattering medium, mimicking skin. It is shown that due to the high coefficients of scattering and absorption of blood the intensity of the reflected radiation decreases directly above the blood vessel, which makes the method applicable for imaging. The question about the optimal position of the radiation source aimed at obtaining the optimal image quality is studied. It is shown that the less noisy and best-quality image is obtained in the case of probing the medium with two sources placed symmetrically with respect to the studied vessel. It is also shown that with increasing depth of the blood vessel embedment the 'blurring' of its image increases almost linearly and is practically independent of the vessel radius in the considered range, which allows one to determine unambiguously the depth of the vessel embedment. The vessel radius may be determined from the peak value of the curve obtained as a result of averaging the vessel image.

Acknowledgements. The work is supported by the Russian Foundation for Basic Research (Grant No. 10-02-01416).

References

1. Gibson A.P., Hebden J.C., Arridge S.R. *Phys. Med. Biol.*, **50**, R1 (2005).
2. Tuchin V.V. *Handbook of Optical Biomedical Diagnostics* (Bellingham: SPIE Press, 2002).
3. Hielscher A.H., Mourant J.R., Bigio I.J. *Appl. Opt*., **36**, 125 (1997).
4. Tuchin V.V. *Lazery i volokonnaya optika v biomeditsinskikh issledovaniyakh* (Lasers and Fibre Optics in Biomedical Studies) (Moscow: Fizmatlit, 2010).
5. Feng S., Zeng F., Chance B. *Appl. Opt.*, **34** (19), 3826 (1995).
6. Fawzi Y.S., Youssef Abo-Bakr M., El-Batanony M.H., Kadah Y.M. *Appl. Opt*., **42** (31), 6398 (2003).
7. Kienle A., Patterson M.S. *J. Opt. Soc. Am. A*, **14** (1), 246 (1997).
8. Kienle A., Patterson M.S., Dognitz N., et al. *Appl. Opt.*, **37** (4), 779 (1998).
9. Prahl S.A., Keijzer M., Jacques S.L., Welch A.J. *SPIE Institute Series*, **IS5**, 102 (1989).
10. Boas D.A., Culver J.P., Stott J.J., Dunn A.K. *Opt. Express*, **10** (3), 159 (2002).
11. Bykov A.V., Priezzhev A.V., Bass L.P., et al. *Proc. SPIE Int. Soc. Opt. Eng.*, **6047**, 604719 (2006).
12. Bykov A.V., Kirillin M.Yu., Priezzhev A.V., in *Handbook of Optical Sensing of Glucose in Biological Fluids and Tissues* (Boca Raton – London – New York: CRC Press, Taylor & Francis Group, 2008) pp 65–95.
13. Bykov A.V., Kirillin M.Yu., Priezzhev A.V. *Kvantovaya Elektron*., **35** (2), 135 (2005) [*Quantum Electron*., **35** (2), 135 (2005)].
14. Fridolin I., Lindberg L-G. *Phys. Med. Biol.*, **45**, 3765 (2000).
15. Liu N., Sassaroli A., Fantini S. *J. Biomed. Opt.*, **10** (5), 051801 (2005).
16. Liu N., Sassaroli A., Zucker M.A., Fantini S. *Opt. Lett*., **30**, 281 (2005).
17. Gratton G., Corballis P.M., Cho E., Fabiani M., Hood D.C. *Psychophysiology*, **32**, 505 (1995).
18. Villringer A., Chance B. *Trends Neurosci.*, **20**, 435 (1997).
19. Robertson C.S., Gopinath S.P., Chance B. *J. Neurotrauma*, **12**, 591 (1995).
20. Kessel B., Jeroukhimov I., Ashkenazi I., et al. *Injury*, **38** (9), 1065 (2007).
21. Troy T.L., Thennadil S.N. *J. Biomed. Opt.*, **6** (2), 167 (2001).
22. Driver I., Feather J.W., King P.R., Dawson J.B. *Phys. Med. Biol.*, **34** (12), 1927 (1989).
23. Flock S.T., Jacques S.L., Wilson B.C., et al. *Lasers in Surgery and Medicine*, **12**, 510 (1992).
24. van Staveren H.G., Moes C.J.M., van Marle J., et al. *Appl.Opt.*, **30**, 4507 (1991).
25. Roggan A., Friebel M., Dorschel K., et al. *J. Biomed. Opt*., **4**, 36 (1999).
26. Gostout C.J., Jacques S.L. *Gastrointestinal Endoscopy*, **41** (3), 218 (1995).
27. Tuchin V.V. *Optical Clearing of Tissue and Blood* (Bellingham: SPIE Press, 2006).